IEEE Photonics Journal
An IEEE Photonics Society Publication

All-Silicon Energy-Efficient Optical Diode Using Opto-Mechanical Microring Resonators

Volume 12, Number 3, June 2020

Linghuan Xu
Li Liu
Miaomiao Chen
Mengyuan Ye

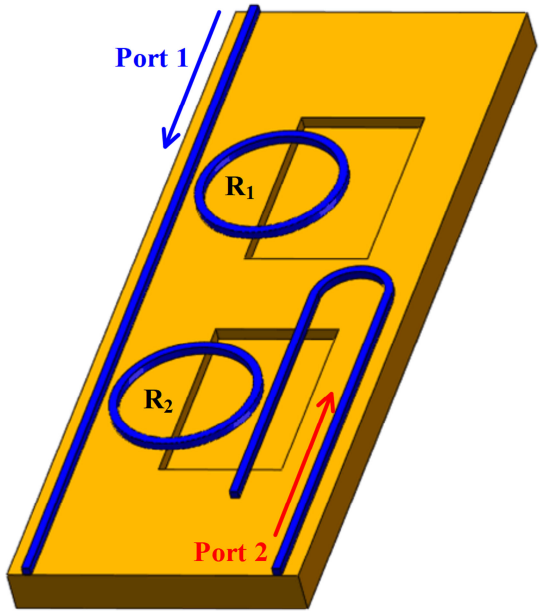

DOI: 10.1109/JPHOT.2020.3000898

All-Silicon Energy-Efficient Optical Diode Using Opto-Mechanical Microring Resonators

Linghuan Xu,[1,2] **Li Liu**,[1,2] **Miaomiao Chen,**[1,2] **and Mengyuan Ye**[1,2]

[1]School of Automation, China University of Geosciences, Wuhan 430074, China
[2]Hubei Key Laboratory of Advanced Control and Intelligent Automation for Complex Systems, Wuhan 430074, China

DOI:10.1109/JPHOT.2020.3000898

Manuscript received May 24, 2020; accepted June 4, 2020. Date of publication June 9, 2020; date of current version June 22, 2020. This work was supported in part by the National Natural Science Foundation of China under Grant 61805215 and in part by Wuhan Municipal Science and Technology Bureau (2019010701011410). Corresponding author: Li Liu (e-mail: liliu@cug.edu.cn).

Abstract: By utilizing two cascaded all-silicon opto-mechanical microring resonators (MRRs), an energy-efficient optical diode with high nonreciprocal transmission ratios (NTRs) is proposed and experimentally realized. The optical diode is composed of an all-pass opto-mechanical MRR and an add-drop opto-mechanical MRR. Due to the largely enhanced interaction between the photons and the suspended structure, the opto-mechanical effect can be dramatically improved. With injecting low optical powers, the optical gradient force can be effectively aroused in the opto-mechanical MRRs, which would arise nanometer scale waveguide deformations and the significant spectrum red-shifts of the rings. The opto-mechanical effect would cause different red-shifts of the two MRR resonances in the forward and backward transmissions, which contributes to realizing the nonreciprocal transmissions. The experimental results show that with -4.2 dBm power consumption, the optical diode can achieve high NTRs approach 41.8 dB. Due to the dominant advantages of complementary metal oxide semiconductor (COMS) compatibility, high NTRs (41.8 dB), low power consumption (-4.2 dBm) and compact size (0.015 mm^2), the device has remarkable applications in on-chip signal processing systems.

Index Terms: Silicon optical diode, low-power consumption, high nonreciprocal transmission ratio, opto-mechanical effect.

1. Introduction

Optical diodes can realize unidirectional optical transmission [1]–[4], which are widely utilized for optical signal processing [5], [6]. Simultaneously, the processing speed and storage capacity of the optical system could be effectively improved [7]–[13]. Various optical diodes have been demonstrated by utilizing the magneto-optical effect. However, due to the disadvantages of the device large size and the incompatibility with complementary metal-oxide semiconductor (CMOS), these optical diodes are hard to be integrated. Furthermore, some optical diodes are realized by space-time modulation [14], indirect inter-band photon transition [15] and photonic crystal fiber [16], whose manipulation are relatively complex.

Recently, silicon-on-insulator (SOI) technology has attracted widespread attention due to its high speed [17], [18], compatibility with CMOS and low power consumption [19]–[22]. In the past decade, many researchers have explored all-silicon optical diodes and made remarkable progress. On the

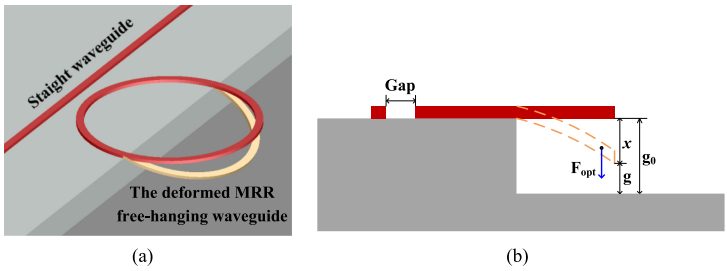

Fig. 1. (a) The structure of the suspended MRR. (b) The deformed waveguide affected by the optical force.

basis of thermo-optic effect, Fan *et al.* and Xu *et al.* realized optical diodes with 40 dB nonreciprocal transmission ratio (NTR) (3.55 dBm power consumption) [23], [24] and 24 dB NTR (8.2 dBm power consumption) [25] respectively based on two cascaded microring resonators (MRRs). However, the power consumption of the thermo-optic effect is relatively high, which cannot meet the requirements of energy-efficient optical systems. Dong *et al.* adopted one suspended racetrack ring and achieved a 12.8 dB NTR at 6 dBm power [26]. To improve performances of the device, Liu *et al.* adopted two cascaded free-hanging MRRs to realize a 33.6 dB NTR at low power consumption of 0.96 dBm [27], but the NTRs are supposed to be improved. Therefore, in the pursuit of low-power optical systems, compact optical diodes with high NTRs ($>$40 dB) and low power consumption (<-3 dBm) are still highly required.

Recently, the opto-mechanical MRRs is a core component in the research of optical communication devices [28]–[30]. With the significant enhancement of the optical field density in the suspended structure, the opto-mechanical effect is greatly improved, which could significantly activate the low-power opto-mechanical effect [31]. The optical gradient force generated between the suspended ring waveguide and the silica substrate could lead to the mechanical deformations of the microring with nanometer or even micrometer level, which causes effective MRR resonance red-shifts [32]–[35]. Consequently, the free-hanging MRRs are competent to efficiently process on-chip optical signals.

In this paper, we proposed and implemented a silicon passive optical diode using cascaded opto-mechanical MRRs with high NTRs and low power consumption. The optical diode consists of a suspended all-pass ring and an add-drop ring. When the optical power is injected from the forward path and backward path respectively, the two MRRs would experience different resonance red-shifts, which leads to the asymmetric transmission spectra. Consequently, in the forward path the optical signal can be transmitted, but blocked in the backward path. The proposed optical diode can experimentally achieve a high NTR approach 42 dB at 1556.89 nm with a low power of -4.2 dBm, which is significant for the on-chip energy-efficient optical signal processing.

2. Operation Principle

As shown in Fig. 1(a), optical gradient force would be generated [36]–[38], due to the enhanced interaction of evanescent waves between the suspended MRR arc and the oxide substrate. Fig. 1(b) illustrates that the initial separation gap between the suspended ring and the substrate is g_0. When a strong enough power is injected into the MRR, the generated optical gradient force F_{opt} can induce a waveguide deformation x of the MRR suspended waveguide. When the optical gradient force quals to the mechanical force, the MRR free-standing arc achieves an equilibrium condition, which causes the MRR spectrum red-shifts. In this case, the separation gap is converted into $g = g_0 - x$.

The generated optical force is given by [33]

$$F_{opt} = -\frac{\partial U}{\partial g} = -\frac{U}{\lambda_r}\frac{\partial \lambda_r}{\partial x} = -\frac{2\tau_e^{-1}P_{in}}{(\lambda_c - \lambda_r)^2\lambda_r^{-3} + \lambda_r\left(\tau_i^{-1} + \tau_e^{-1}\right)^2}\frac{\partial \lambda_r}{\partial x} \tag{1}$$

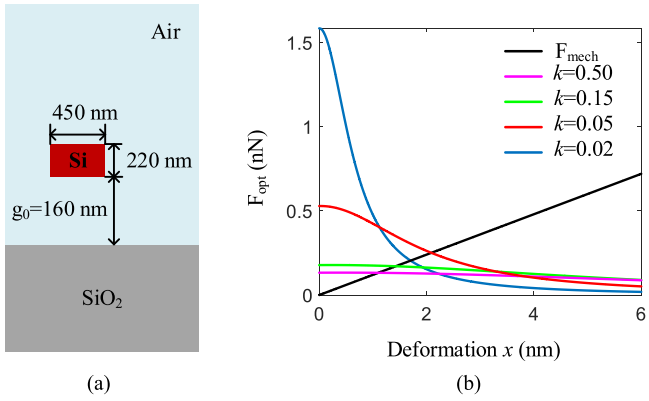

Fig. 2. (a) The schematic image of the free-standing arc. (b) The waveguide deformation under different coupling coefficients.

where P_{in} represents the input power of λ_c which denotes the control light wavelength, λ_r is the MRR resonant wavelength, τ_i^{-1} is caused by the loss of the internal cavity (the intrinsic decay rate) and τ_e^{-1} is the extrinsic decay rate, which could be denoted by

$$\tau_e^{-1} = -\frac{In(1-k)C}{2\pi R n_{eff}} \tag{2}$$

where R is the opto-mechanical MRR radius, k represents the coupling coefficient, C represents the light speed and n_{eff} is the ring effective index. Based on the designed device parameters, the extrinsic decay rate τ_e^{-1} is 3.45×10^{10}.

The red-shift $\delta\lambda$ of the microring could be expressed as

$$\delta\lambda \propto \frac{g_{om}^2 P_{in}}{k_{mech}} \tag{3}$$

where $g_{om} = \frac{\partial n_{eff}}{\partial g}$ is the tuning efficiency of the opto-mechanical effect, and k_{mech} is the mechanical spring constant of the opto-mechanical MRR.

We design the MRR-based optical diode on an SOI wafer which is commonly used to fabricate silicon nano-mechanical devices. The SOI wafer is composed of 220-nm-thick silicon in the top layer and 2-μm-thick SiO_2 substrate. To reduce the bending loss, the radius of the MRR is chosen as 30 μm. Firstly, in order to ensure single mode transmission, Fig. 2(a) shows that the waveguide width is set to 450 nm. Secondly, the coupling coefficient k between the straight waveguide and the MRR is optimized to achieve the strongest opto-mechanical effect. Fig. 2(b) illustrates that when the optical force (the colored curve) balances the mechanical force (the black line), namely $F_{opt}(x) + k_{mech}x = 0$, the free-hanging waveguide arc reaches an equilibrium shape. Different coupling coefficients ($k =$ 0.5, pink curve; $k = 0.15$, green curve; $k = 0.05$, red curve and $k = 0.02$, blue curve) are selected to calculate the relationship between the generated optical force and mechanical deformation. When k is set to 0.05, the opto-mechanical effect could induce the largest deformation which corresponds to the highest resonance red-shift. Thirdly, the separation gap g_0 is also a key factor to enhance the optical force. On one hand, a smaller separation gap contributes to a stronger optical force. On the other hand, the width of the waveguide limits the minimum value of the separation gap g_0. According to the practical fabrication technology, g_0 should be about half the waveguide width. Under the above analysis, the separation height g_0 is set as 160 nm [29]. Finally, the suspended waveguide length is 11.2 μm due to the MRR radius of 30 μm and the mechanical structure limitation.

Fig. 3(a) illustrates that the effective refractive indexes gradually reduce with increasing the separation gap. From the relationship between the resonant wavelength and the effective refractive index, the resonant red-shift under different waveguide deformations can be calculated, as shown

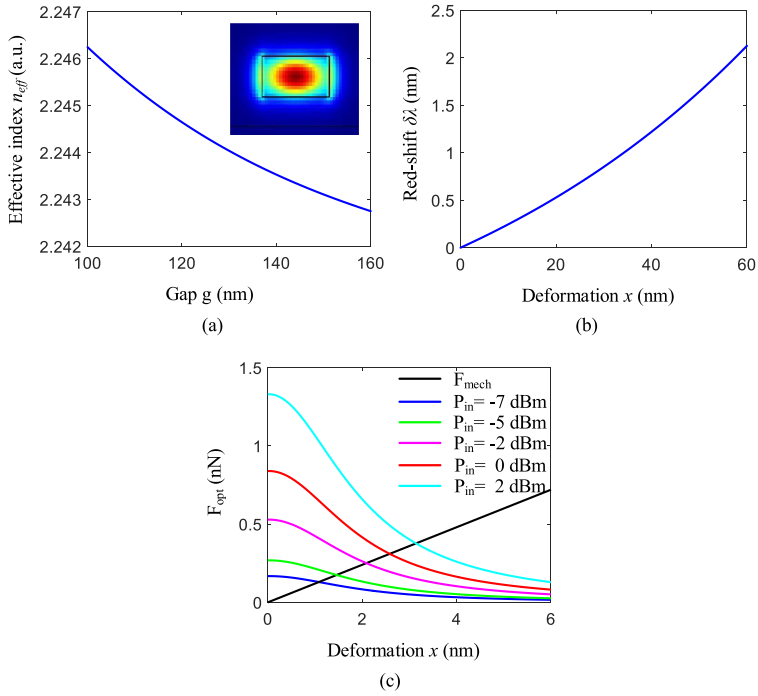

Fig. 3. (a) The effective indexes under different separation gaps. (b) The resonance red-shifts under different waveguide deflections. (c) The generated force under different deflections.

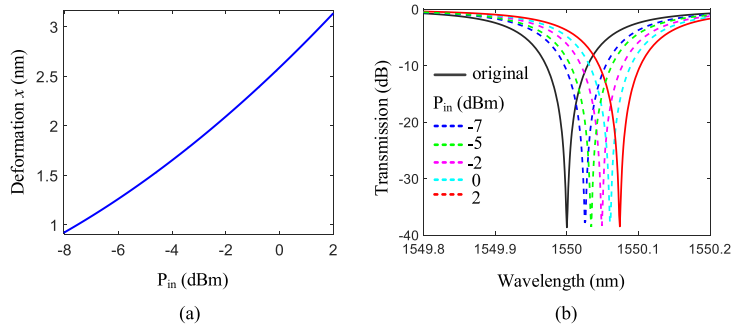

Fig. 4. (a) The deflection of suspended MRR with adjusting the input powers. (b) The transmission of the all-pass opto-mechanical MRR at different input powers.

in Fig. 3(b). The red-shift of the MRR resonance could realize 0.0605 nm with a waveguide deformation of 2.585 nm. By using Eqs. (1)-(3) and the designed device parameters, Fig. 3(c) shows the obtained optical forces with different input powers. When the generated optical gradient force (the colored curve) balances the mechanical force (the black line), namely $F_{opt}(x) + k_{mech}x = 0$, the free-hanging arc would obtain an equilibrium level. As the input optical power increases, the corresponding deformation x of the balance position would be larger. Therefore, by controlling the operation powers, the transmission spectrum of the MRR can be effectively adjusted.

Fig. 4(a) illustrates the deformation of opto-mechanical MRR under various resonance powers (i.e. 1550 nm). Obviously, the deformation x increases with the input powers. By combining the simulation results in Fig. 3(b) and Fig. 4(a), the transmissions of the all-pass MRR under different operation optical powers can be obtained, as shown in Fig. 4(b). The original transmission spectrum of the all-pass MRR is shown as the black line. With injecting input powers of -7 dBm, -2 dBm, 0 dBm and 2 dBm, the transmission spectra of the all-pass MRR are effectively shifted with

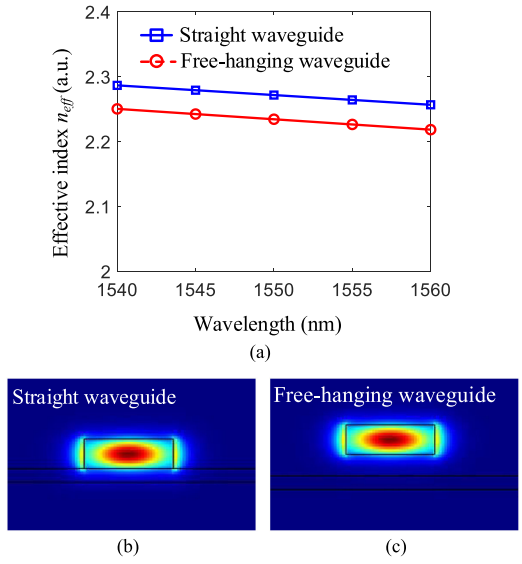

Fig. 5. (a) Effective refractive index versus wavelength. Energy profiles of the fundamental modes in (b) straight waveguide and (c) free-hanging waveguide, respectively.

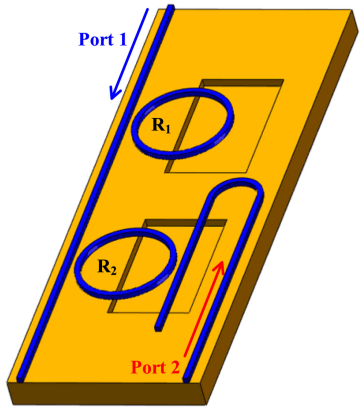

Fig. 6. The nonreciprocal device structure.

0.02545 nm (the blue curve), 0.04873 nm (the purple curve), 0.0605 nm (the blue curve), and 0.0738 nm (the red curve), respectively.

To optimize the waveguide effective indexes between different components, the FDTD (finite-difference time-domain) Solutions are utilized to analyze the energy profiles of suspended MRR waveguide and the straight waveguide. Fig. 5(a) shows the effective indexes of the suspended ring waveguide and the straight waveguide are 2.24 and 2.27 at 1550 nm, respectively. Therefore, the effective index difference between the above different waveguides can be ignored, which facilitates the light transmission and coupling. Figs. 5(b) and 5(c) show the fundamental modes in the straight waveguide and suspended waveguide, respectively.

3. Results and Discussion

3.1 Simulation Results

Fig. 6 shows that the optical diode is composed of a suspended all-pass MRR (i.e. R_1) and an add-drop MRR (i.e. R_2) with the same radius of 30 μm. The forward direction is from port 1 to port 2 while the backward direction is from port 2 to port 1. The silicon slab heights and the waveguide

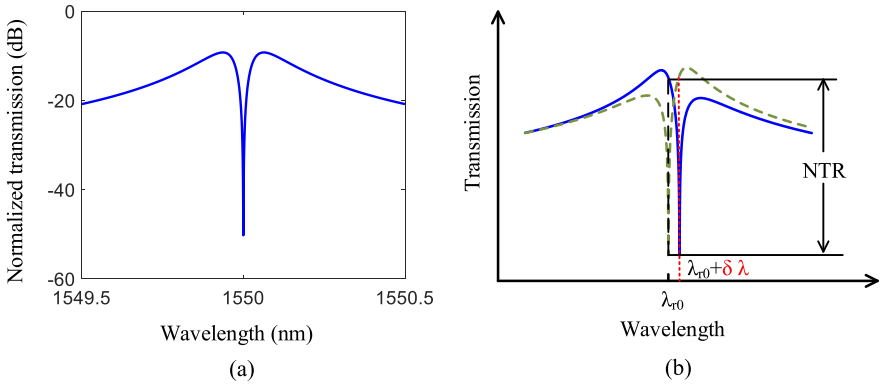

Fig. 7. (a) The original normalized device transmission spectrum. (b) The forward spectrum (the blue solid curve) and the backward spectrum (the green dashed curve) of the nonreciprocal device.

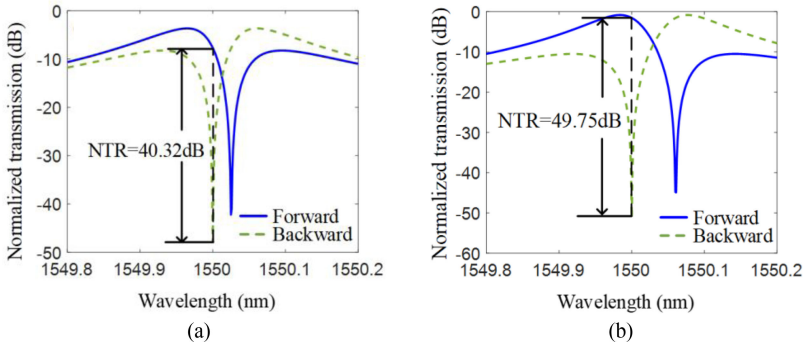

Fig. 8. The normalized transmissions with injecting powers of (a) −7 dBm, (b) 0 dBm, respectively.

widths of the rings and the bus waveguide are set to 220 nm and 450 nm, respectively. The vertical separation height g_0 between the suspended MRR waveguide and the silica substrate is optimized as 160 nm, and the suspended waveguide length is set to 11.2 μm.

Fig. 7(a) shows the initial transmission spectrum of the cascaded free-hanging MRRs. The operation wavelength is set at λ_{r0}, which is the aligned resonant wavelength of the two rings (i.e. 1550 nm). Fig. 7(b) illustrates the forward transmission spectrum of the optical diode as the blue solid line and the backward transmission as the green dashed line. Forward transmission (the blue curve): the input power P_{in} is injected from port 1. As the input wavelength is set as λ_{r0}, the input power could couple into R_1 and accumulate to a high level, which is strong enough to excite the opto-mechanical effect and cause waveguide deformation. Thus, the resonance of R_1 would shift with a wavelength of $\delta\lambda$. Because the optical power is attenuated by R_1, the remaining power almost has no influence on R_2. In this case, the optical signal could transmit in the forward direction. Backward transmission (the green curve): the same input power is injected from port 2. As the input light firstly arrives at R_2, the transmission spectrum of R_2 will shift with $\delta\lambda$ because of the nonlinear effect. Hence, the major optical power cannot be coupled into R_2. Namely, the signal cannot reach port 1. Therefore, the optical signal can be forward transmitted and backward blocked, and a high NTR at the input wavelength of λ_{r0} could be achieved.

Firstly, the operation power is adjusted to −7 dBm. In the forward transmission, the resonance of microring R_1 would shift with 0.02545 nm while the spectrum of R_2 remains unchanged. Consequently, the transmission of the optical diode is shown as the blue solid curve in Fig. 8(a). In contrast, due to the 0.02545 nm red-shift of R_2, the transmission of the backward transmission is

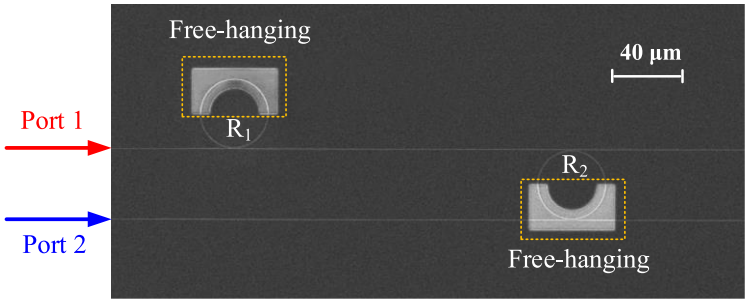

Fig. 9. SEM image of the fabricated nonreciprocal diode.

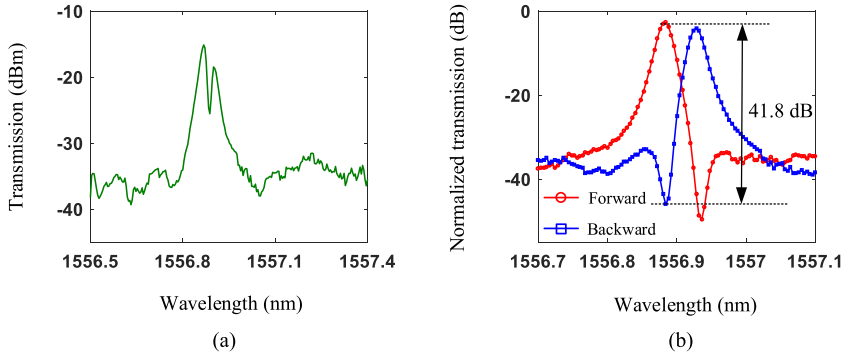

Fig. 10. (a) Original transmission of the silicon diode. (b) Measured transmissions of the forward direction and backward direction by inputting an operation power of −4.2 dBm.

illustrated as the green dashed curve. It is clear that an NTR of 40.32 dB could be achieved. Finally, the operation power is adjusted to 0 dBm and the highest NTR of 49.75 dB could be obtained.

3.2 Experimental Results

We fabricate the MRR-based optical diode on a commercial SOI wafer (220-nm-thick silicon in the top layer and 3-μm-thick SiO_2 substrate). The suspended structures of the opto-mechanical MRRs were released by dry etching procedures (for Si etching) which include E-beam lithography (EBL) and inductively coupled plasma (ICP), and a hydrofluoric (HF) wet etching procedure (for SiO_2 etching). Firstly, the device pattern was transferred to the photoresist by the first EBL and then etched 195 nm downward by the first ICP. Secondly, half of each MRR was etched another 25 nm downward by the second EBL and ICP. As a result, half of each MRR oxide substrate was exposed to the air (i.e., the released region), while the other half of the oxide substrate had a 25-nm-thick silicon protective layer. Finally, we used the HF acid to selectively remove the silica substrate in the released area to control the depth of the separation gap g_0. In this case, the waveguides corresponding to the above half ring would be suspended. On the contrary, the other waveguides were fixed. Fig. 9 shows the scanning electron microscope (SEM) image of the device, and the yellow boxes illustrate the suspended MRR structure. The radii of the two MRRs are about 20 μm, and their waveguide widths are 450 nm which are the same as the straight waveguides. The forward transmission of the silicon diode is from port 1 to port 2 and the backward path is the opposite.

The initial transmission spectrum of the silicon diode is measured in Fig. 10(a). The resonant wavelengths of the two rings are approximately 1556.89 nm. To research the characteristics of the nonreciprocal transmissions, continuous wave (CW) light is injected into the device whose operation wavelength is fixed at 1556.89 nm. In the meantime, we utilize a low-power amplified spontaneous emission (ASE) source to measure the transmission spectrum of the optical diode.

TABLE 1
Experimental Results of Optical Diodes Based on Silicon MRRs

Reference	Required power (dBm)	NTR (dB)
[23]	3.2	27
[24]	3.55	40
[25]	8.2	24
[26]	6	12.8
[27]	0.96	33.6
This work	-4.2	41.8

Fig. 10(b) shows the forward transmission spectrum (the red curve) and the backward transmission spectrum (the blue curve) of the silicon device by injecting a low optical power of −4.2 dBm, which illustrates that a high NTR of 41.8 dB could be achieved. In the future, the NTRs of the silicon diode could be largely improved by designing the two MRRs at the critical coupling. In this case, the extinction ratios of the two MRRs can be significantly increased, which facilitates the achievement of higher NTRs.

Table 1 illustrates a comparison of recent performance (NTRs and the power consumption) of silicon MRR-based optical diodes. Although the schemes of cascaded MRRs could achieve NTRs of 27 dB [23], 40 dB [24] and 24 dB [25], their power consumptions are relatively high, which are unfavorable to meet the requirements of energy-efficient signal processing. By using a single racetrack MRR, not only is the NTR relatively low as 12.8 dB, but also it requires 6 dBm input power [26]. The scheme of cascaded all-pass MRRs achieves an improvement in performance. However, the NTR (33.6 dB) and the consumption (0.96 dBm) are still required to be further improved [27]. Compared with the above devices, the proposed optical diode could experimentally realize a high NTR (41.8 dB) with a low power consumption (−4.2 dBm), which has widely broad applications in on-chip optical communication systems.

4. Conclusions

In conclusion, an ultra-low power optical diode with high NTRs by utilizing the silicon cascaded free-hanging MRRs has been experimentally realized. The operation principle is based on the optical force in the suspended MRRs, whose spectrum characteristics can be flexibly controlled by ultra-low input powers. By using the finely designed asymmetric structure, high NTRs of 41.8 dB could be achieved under the low input powers of −4.2 dBm. The compact optical diode with high NTR, ultra-low power consumption and CMOS compatibility could be widely used in on-chip optical systems.

References

[1] Y. Han, Z. Yu, Y. Liu, and Z. Chen, "Realization of compact broadband optical diode in linear air-hole photonic crystal waveguide," *Opt. Exp.*, vol. 24, no. 21, pp. 24592–24599, 2016.
[2] B. Shen, R. Polson, and R. Menon, "Integrated digital metamaterials enables ultra-compact optical diodes," *Opt. Exp.*, vol. 23, no. 8, pp. 10847–10855, 2015.
[3] S. Takanori, T. Fujisawa, and K. Saitoh, "All-optical diode suppressing broadband backward transmission using single- and four-port photonic crystal cavities," *IEEE Photon. J.*, vol. 11, no. 1, Feb. 2019, Art no. 4900214.
[4] V. F. Nezhad, A. Haddadpour, and G. Veronis, "Tunable spatial mode converters and optical diodes for graphene parallel plate waveguides," *Opt. Exp.*, vol. 24, no. 21, pp. 23883–23897, 2016.

[5] G. S. B. Filho, F. L. B. Martins, M. F. Junior, A. A. R. Araujo, J. C. Nascimento, and A. G. Coelho, "All-optical logic gates and boolean expressions in a photonic mach-zehnder interferometer," *J. Opt. Commun.*, vol. 40, no. 1, pp. 7–16, 2019.
[6] C. Husko, T. D. Vo, B. Corcoran, J. Li, T. F. Krauss, and B. J. Eggleton, "Ultracompact all-optical XOR logic gate in a slow-light silicon photonic crystal waveguide," *Opt. Exp.*, vol. 19, no. 21, pp. 20681–20690, 2011.
[7] R. Baets *et al.*, "An ultra-small, low-power, all-optical flip-flop memory on a silicon chip," *Nature Photon.*, vol. 4, no. 3, pp. 182–187, 2010.
[8] D. A. B. Miller, "Are optical transistors the logical next step?" *Nature Photon.*, vol. 4, no. 1, pp. 3–5, 2010.
[9] L. Liu, J. Dong, and X. Zhang, "Chip-integrated all-optical 4-bit Gray code generation based on silicon microring resonators," *Opt. Exp.*, vol. 23, no. 16, pp. 21414–21423, 2015.
[10] S. Lechago, C. Garcia-Meca, A. Griol, M. Kovylina, L. Bellieres, and J. Marti, "All-silicon on-chip optical nanoantennas as efficient interfaces for plasmonic devices," *ACS Photon.*, vol. 6, no. 5, pp. 1094–1099, 2019.
[11] K. Xu, "Monolithically integrated Si gate-controlled light-emitting device: science and properties," *J. Opt.*, vol. 20, no. 2, 2018, Art. no. 02401.
[12] M. M. Gupta, and S. Medhekar, "Three-port asymmetric (three-port ordered-route) light transmission in a linear, time-independent and non-magnetic structure of photonic crystals," *Epl*, vol. 113, no. 3, 2016, Art. no. 34004.
[13] L. Liu, W. Xue, and Y. Jin, "Photonic approach for microwave frequency measurement using a silicon microring resonator," *IEEE Photon. Technol. Lett.*, vol. 31, no. 2, pp. 153–156, Jan. 2019.
[14] T. Mizumoto, R. Takei, and Y. Shoji, "Waveguide optical isolators for integrated optics," *IEEE J. Quantum Electron.*, vol. 48, no. 2, pp. 252–260, Feb. 2012.
[15] Z. Yu and S. Fan, "Optical isolation based on nonreciprocal phase shift induced by interband photonic transitions," *Appl. Phys. Lett.*, vol. 94, no. 17, pp. 171116-1–171116-3, 2009.
[16] M. S. Kang, A. Butsch, and P. St. J. Russell, "Reconfigurable light-driven opto-acoustic isolators in photonic crystal fibre," *Nature Photon.*, vol. 5, no. 9, pp. 549–553, 2011.
[17] L. Liu, and X. Liu, "All-optical tunable microwave filter with ultra-high peak rejection and low-power consumption," *Opt. Exp.*, vol. 28, no. 9, pp. 13455–13465, 2020.
[18] L. Liu, S. Liao, W. Xue, and J. Yue, "Tunable all-optical microwave filter with high tuning efficiency," *Opt. Exp.*, vol. 28, no. 5, pp. 6918–6928, 2020.
[19] R. A. Soref, "The past, present and future of silicon photonics," *IEEE J. Sel. Top. Quantum Electron.*, vol. 12, no. 6, pp. 1678–1687, Nov.-Dec. 2006.
[20] B. Jalali and S. Fathpour, "Silicon photonics," *J. Lightw. Technol.*, vol. 24, no. 12, pp. 4600–4615, Dec. 2006.
[21] J. Leuthold, C. Koos, and W. Freude, "Nonlinear silicon photonics," *Nature Photon.*, vol. 4, no. 8, pp. 535–544, 2010.
[22] L. Liu, H. Qiu, Z. Chen, and Z. Yu, "Photonic measurement of microwave frequency with low-error based on an optomechanical microring resonator," *IEEE Photon. J.*, vol. 9, no. 6, Dec. 2017, Art no. 5503611.
[23] L. Fan *et al.*, "An all-silicon passive optical diode," *Sci.*, vol. 335, no. 6067, pp. 447–450, 2012.
[24] L. Fan, L. T. Varghese, J. Wang, Y. Xuan, A. M. Weiner, and M. Qi, "Silicon optical diode with 40 dB nonreciprocal transmission," *Opt. Lett.*, vol. 38, no. 8, pp. 1259–1261, 2013.
[25] M. Xu, J. Wu, T. Wang, X. Hu, X. Jiang, and Y. Su, "Push-pull optical nonreciprocal transmission in cascaded silicon microring resonators," *IEEE Photon. J.*, vol. 5, no. 1, Feb. 2013, Art. no. 2200307.
[26] H. Qiu, J. Dong, L. Liu, and X. Zhang, "Energy-efficient on-chip optical diode based on the optomechanical effect," *Opt. Exp.*, vol. 25, no. 8, pp. 8975–8985, 2017.
[27] L. Liu, J. Yue, X. Fan, and W. Xue, "On-chip passive optical diode with low-power consumption," *Opt. Exp.*, vol. 26, no. 25, pp. 33463–33472, 2018.
[28] L. Liu, Y. Yang, Z. Li, X. Jin, W. Mo, and X. Liu, "Low power consumption and continuously tunable all-optical microwave filter based on an opto-mechanical microring resonator," *Opt. Exp.*, vol. 25, no. 2, pp. 960–971, 2017.
[29] H. Cai *et al.*, "A nanoelectromechanical systems optical switch driven by optical gradient force," *Appl. Phys. Lett.*, vol. 102, no. 2, 2013, Art. no. 023103.
[30] D. Van Thourhout and J. Roels, "Optomechanical device actuation through the optical gradient force," *Nat. Photon.*, vol. 4, no. 4, pp. 211–217, 2010.
[31] H. Liu, M. Panmai, Y. Peng, and S. Lan, "Optical pulling and pushing forces exerted on silicon nanospheres with strong coherent interaction between electric and magnetic resonances," *Opt. Exp.*, vol. 25, no. 11, pp. 12357–12371, 2017.
[32] M. Wang, H. Li, D. Gao, L. Gao, J. Xu, and C. Qiu, "Radiation pressure of active dispersive chiral slabs," *Opt. Exp.*, vol. 23, no. 13, pp. 16546–16533, 2015.
[33] L. Liu *et al.*, "Low-power all-optical microwave filter with tunable central frequency and bandwidth based on cascaded opto-mechanical microring resonators," *Opt. Exp.*, vol. 25, no. 15, pp. 17329–17342, 2017.
[34] M. Ren *et al.*, "Nano-optomechanical Actuator and Pull-Back Instability," *ACS Nano*, vol. 7, no. 2, pp. 1676–1681, 2013.
[35] L. Liu, W. Xue, X. Jin, J. Yue, Z. Yu, and L. Zhou, "Bandwidth and wavelength tunable all-optical filter based on cascaded opto-mechanical microring resonators," *IEEE Photon. J.*, vol. 11, no. 1, Feb. 2019, Art. no. 7800210.
[36] J. Tao, J. Wu, H. Cai, Q. Zhang, J. M. Tsai, J. Lin, and A. Liu, "A nanomachined optical logic gate driven by gradient optical force," *Appl. Phys. Lett.*, vol. 100, no. 11, 2012, Art. no. 113104.
[37] L. Liu, Y. Yang, J. Yue, and S. Liao, "On-chip low-power Gray code generation based on opto-mechanical microring resonators," *IEEE Photon. J.*, vol. 12, no. 3, Jun. 2020, Art. no. 4500312.
[38] M. Chen, L. Liu, L. Xu, M. Ye, X. Jin, and Z. Yu, "On-Chip all-optical tunable filter with high tuning efficiency," *IEEE Photon. J.*, vol. 12, no. 2, Apr. 2020, Art. no. 7800510.